## PAPER

Check for updates

# Unlocking branched cutin *via* sudden supercritical water hydrolysis of tomato peel†

Vesna Leontijevic,[a,b] Danilo Cantero,[a,b] Suset Barroso Solares, [ID][c,d] Antonio Heredia Bayona[e] and María José Cocero Alonso [ID] *[a,b]

This study presents a novel approach to unlock and enrich branched cutin from tomato peel waste using sudden supercritical water hydrolysis. Cutin, the structural polyester of the plant cuticle, offers exceptional properties for biomaterials developments, however, conventional extraction methods often degrade its intricate three-dimensional network, limiting its potential applications. Utilizing sudden supercritical water hydrolysis (SCWH) with a reaction time of approximately one second, non-cutin components are hydrolyzed while preserving and enriching the native cutin structure. Characterization of the cutin-rich solid revealed the absence of a detectable glass transition temperature or melting point, indicating the maintenance of its native polymeric architecture phenomena typically observed when cutin is isolated as a mixture of monomers. Furthermore, mechanical testing revealed high rigidity under more stringent conditions, with a measured Young's modulus of 0.7 GPa. This rapid and efficient process not only valorizes agricultural and industrial residues but also enables the development of sustainable, bio-based materials. The successful preservation and enrichment of native cutin open new avenues for its application in advanced biomaterials, offering a promising alternative to fossil fuel-derived polymers.

**Green foundation**

1. The manuscript provides new knowledge about reactions occurring in water at high pressure and temperature. The change of physical properties with pressure and temperature opens the opportunity to operate with non-polar compounds using water as solvent and reaction medium.

2. The work provides a significant increase in the understanding of the behaviour of the ester bonds of polyesters when operating under supercritical water conditions.

3. A continuous process for obtaining native cutin biopolyester while preserving its branched polyester structure intact. This process uses only water and operates in under 1.5 seconds, allowing for low-volume, easily scalable reactors. In future work the availability of native cutin facilitates a deeper understanding of its structure and depolymerization products.

## 1. Introduction

Cutin is a major structural component of the plant cuticle – the protective outer layer of aerial plant parts.[1] It is a branched

*[a]PressTech group, BioecoUva Research Institute of Bioeconomy, University of Valladolid, Valladolid 47011, Spain. E-mail: mariajose.cocero.alonso@uva.es*
*[b]Chemical Engineering and Environmental Technology Department, EII Sede Mergelina, University of Valladolid, Valladolid 47011, Spain*
*[c]Archaeological and Historical Materials (AHMAT) Group, BioEcoUVA Research Institute on Bioeconomy, University of Valladolid (UVa), Valladolid, 47011, Spain*
*[d]Condensed Matter Physics, Crystallography, and Mineralogy Department, Faculty of Science, University of Valladolid, Valladolid 47011, Spain*
*[e]IHSM-UMA-CSIC, Departamento de Biología Molecular y Bioquímica, Facultad de Ciencias, Campus de Teatinos University of Malaga, 29071 Málaga, Spain*
†Electronic supplementary information (ESI) available. See DOI: https://doi.org/10.1039/d5gc00375j

polyester composed of C16, C18 hydroxy, or epoxy fatty acids linked by ester bonds. In nature, cutin forms an amorphous, resistant, flexible, insoluble, infusible, and chemically inert polymeric network, which acts as a barrier.[2,3] Its unique thermal properties, such as high specific heat and glass transition temperature, allow it to transition fluidly between rigid and viscous stages depending on temperature. Moreover, cutin exhibits viscoelastic behavior characteristic of a polymer network,[4,5] markedly different industrially favored polymers like polyhydroxyl alkenoates (PHA) or other thermoplastic linear polyesters synthesized through chemical or enzymatic polymerizations.

The cuticle also contains hydrophobic compounds known as waxes, which are categorized as intracuticular (within the cutin matrix) and epicuticular (on the cuticle surface).[3] Additionally, the cutin matrix contains phenolic compounds,

primarily hydroxycinnamic acid derivatives and flavonoids,[6] which may influence its properties and potential applications.

The plant cuticle protects the epidermis of the aerial plant, acting as a barrier against environmental stresses. It prevents desiccation by minimizing water loss, regulates gas exchange, facilitates the transport of lipophilic substances, attenuates UV radiation, and mediates biotic interactions.[5,7] In the context of decreasing water availability and climate change, understanding the cuticle's properties is essential for developing sustainable agricultural practices and novel materials that leverage cutin's inherent functionalities.

Tomato (*Solanum lycopersicum*) is the second-largest vegetable crop globally, with a production of 254.5 million tons in 2022.[8] The processing of tomatoes into products like ketchup, paste, purée, sauce, or juice generates significant byproducts – collectively known as tomato pomace – which accounts for 10–30% w/w of the manufacturing weight.[9] Tomato pomace consists mainly of peels, seeds, and residual pulp. While some tomato pomace is used in animal feed manufacturing due to its dietary fiber content,[10] large quantities remain underutilized, presenting a waste disposal challenge. Upcycling this residue could reduce environmental impact and create additional revenue streams.

Chemically, tomato seeds are rich in essential amino acids, minerals (iron, manganese, zinc, and copper), and mono-unsaturated fatty acids like oleic acid. On the other hand, tomato peels are abundant in carotenoids, lycopene,[11] and notably, cutin – constituting up to 80% of the peel.[12] The cutin in tomato peels predominantly consists of C16 dihydroxy carboxylic acid (over 50%).[13] Additionally, the peels contain approximately 15% w/w polysaccharides (cellulose, hemicellulose, and pectin) from the epidermal cell walls.[14]

Conventional methods for isolating cutin involve lengthy, multi-step procedures, including dewaxing and enzymatic hydrolysis to remove polysaccharides or alkaline hydrolysis at 100–120 °C. These processes are time-consuming (hours to days), require additional separation steps, and necessitate the neutralization of reactants used in alkaline hydrolysis. Furthermore, they often yield a small amount of product suitable only for laboratory-scale applications and chemical analysis. The harsh conditions of alkaline hydrolysis can lead to complete hydrolysis of ester bonds, resulting in a mixture of fatty hydroxy acid monomers and compromising the native, branched structure of cutin. Consequently, the intrinsic properties of native cutin remain poorly understood and underexploited.

In this work, we introduce a rapid and efficient method to extract and enrich native cutin from tomato peel waste using sudden supercritical water (SCWH). This technique leverages the unique properties of water under supercritical conditions to selectively hydrolyze non-cutin components within an ultra-short reaction time (~1 second). Water above its critical point (374 °C, 22.1 MPa) exhibits properties significantly different from the ones at ambient conditions, such as low viscosity, high diffusivity, and decreased dielectric constant similar to non-polar organic solvents, facilitate penetration into the biomass structure.[15,16] These characteristics enhance penetration into biomass and solubilization of organic compounds. Additionally, the ionic product of water is reduced at supercritical conditions disfavouring ionic reactions and favoring free radical ones,[17] which can be harnessed to preserve the ester bonds in cutin. Previous studies conducted by our team have demonstrated that carbohydrate hydrolysis exhibits rapid kinetics under supercritical conditions, with reactions occurring on the millisecond timescale. Under these conditions, carbohydrates, being among the most labile components of biomass, undergo hydrolysis rapidly. Specifically, cellulose is initially hydrolyzed into oligomers, which are subsequently converted to glucose.[18] In contrast, biomass components such as lignin require significantly longer reaction times for substantial conversion. Similarly, the cleavage of ester bonds in compounds such as triglycerides also necessitates prolonged reaction durations. In both cases, reaction times exceeding one second are typically required to achieve meaningful bond cleavage and overall conversion.[16,19,20] These observations underscore the potential for achieving high selectivity through precise control of reaction parameters, including temperature, pressure, and reaction time. Further, concerning the energy demands associated with operations under supercritical water (SCW) conditions, prior research has shown that integrating SCWH with a gas turbine can yield a self-sustaining energy system.[21]

This method offers a clean and sustainable approach for biomass fractionation and valorization, previously applied by our team to lignocellulosic biomass[15,20,22] and suberin-lignin composites.[23] By fine-tuning pressure and temperature, we optimize the process to maintain the native, branched structure of cutin, overcoming the limitations of conventional extraction methods. Moreover, the application of green technologies, such as supercritical water hydrolysis (SCWH), for the valorization of biomass like grape seeds has been demonstrated to align with the 12 principles of green engineering.[20,24] A comparable approach can be extended to the processing of tomato peels considering that both biomasses are agricultural residues (waste) from other processing industries.

Recent literature has underscored the importance of green, high-pressure fluid technologies for sustainably extracting and refining biopolymers from agro-food residues. In particular, sub- and supercritical $CO_2$ have emerged as valuable media to enhance mass transfer, preserve polymeric structures, and reduce the formation of undesired byproducts. As highlighted in one review, carbon dioxide plays a dual role under sub- or supercritical conditions: it functions both as a solvent and as an *in situ* acid catalyst through carbonic acid formation, thereby facilitating rapid hydrolysis in "biorefinery" applications without the drawbacks of strong mineral acids.[25]

Likewise, complementary work on pre-treatment and extraction methods demonstrates that subcritical-water processing, $CO_2$-assisted hydrothermal approaches, and enzymatic treatments can effectively break down biomass or food-waste fractions under relatively mild conditions. These techniques aim

**Table 1** Functional properties of native cutin and associated potential applications, adapted from literature[7]

| Property | Component | Function | Potential applications for cuticle/native cutin |
|---|---|---|---|
| Permeability | Intra(*epi*)waxes | Reduce water loss from tissues | **High-barrier materials** for packaging and coatings; extends post-harvest life of plant-based foods; fosters more effective agrochemical uptake |
| Hydration | Polysaccharides, waxes | Absorb water, reduce excess water uptake | **Bioprotective surfaces** to maintain controlled moisture environments in agricultural and food applications |
| Light | Phenolics/flavonoids, epicuticular waxes | Absorb UV-VIS radiation, reflect visible/infrared light | **UV-protective films** and coatings; color-stable, light-reflective surfaces for consumer goods |
| Biomechanics | Polysaccharides, phenolics, waxes | Increase mechanical stiffness; protect against fruit cracking, pest attacks, and herbivores; enable normal epidermal development | **Bio-based composite materials** with enhanced mechanical resilience; biodegradable films for pest management; stronger horticultural products |
| Thermal | Cutin, waxes | Thermo-regulative action | **Thermally stable coatings** for high-temperature applications; improved shelf-life in packaging where temperature fluctuations are a concern |
| Gas exchange | Phenolics/cutin/waxes | Control gas permeability ($CO_2$, $O_2$) | **Ultra-high barrier polymers** for modified-atmosphere packaging; potential integration in 3D bioprinting scaffolds requiring gas regulation |
| Self-cleaning | Epicuticular waxes, cutin | Surfaces remain clean and dry (lotus effect) | **Stain-resistant textiles** and coatings; self-cleaning architectural materials (*e.g.*, roof tiles, building exteriors) |
| Surface glossiness | Epicuticular waxes, cutin | Impart shine/brightness | **Decorative finishes** and glossy coatings for consumer products (furniture, automotive, *etc.*); fruit cosmetic appeal in post-harvest storage |

to retain native structural features, such as ester linkages, while limiting energy consumption and chemical usage.[26] In the context of our supercritical water hydrolysis (SCWH) studies, this body of research supports our strategy of operating under carefully controlled high-pressure conditions to obtain native cutin. Our method thus integrates well with the broader "green chemistry" objectives described in these reviews, providing a robust and selective approach that aligns with established enzymatic or $CO_2$-based methodologies while targeting higher yields and minimal byproduct formation.

By contrast, traditional alkaline hydrolysis of tomato skin cutin results in the destruction of its polyester architecture, as the ester bonds are cleaved into acidic monomers. In other words, the alkaline route converts cutin into smaller molecules rather than preserving its native polymeric structure. An initial attempt to obtain intact (non-hydrolyzed) cutin employed ionic liquid-based hydrolysis in batch mode; however, this approach required prolonged processing times and did not entirely avoid partial cleavage of ester links.[13] In contrast, enzymatic hydrolysis of the accompanying carbohydrates has proven helpful for isolating individual tomato cuticles with minimal damage to the cutin network.[12] Nevertheless, enzymatic methods can demand up to three weeks of laboratory-scale hydrolysis, primarily for characterization purposes.

Furthermore, biosynthetic studies of plant-derived compounds, such as terpenoids, together with modern bioengineering technologies can provide more sustainable and efficient paths to large-scale production.[27] Although considerable progress has been made in elucidating the cutin biosynthetic pathway, experts emphasize that a key barrier is the lack of detailed structural information on native cutin.[28,29] Ensuring an abundant supply of unaltered cutin is thus vital for advancing our understanding of its polymeric architecture

and, ultimately, opening more sophisticated avenues in bioengineering applications.

The availability of native cutin presents compelling opportunities for the development of advanced materials that emulate the functional properties of plant cuticles. Potential applications include bioactive materials for biological pest control, UV-Vis radiation shielding, and cutin-derived matrices well-suited for biomedical devices and 3D bioprinting technologies.[7] In Table 1 (adapted from literature), we outline how specific properties of native cutin, such as its permeability, mechanical resilience, and surface characteristics, could be harnessed to create novel high-barrier polymers, self-cleaning surfaces, thermo-regulative coatings, and other specialty products. Such innovations, made possible by preserving the native structure of cutin, have the potential to expand the utility of naturally derived biomaterials across various industries and cutin-derived materials tailored for biomedical devices and 3D bioprinting technologies.

The objective of this study is to demonstrate the effectiveness of SCWH in extracting and enriching branched, native cutin from tomato peel waste, preserving its three-dimensional structure. We compare our results with conventional alkaline hydrolysis methods, highlighting the advantages of SCWH in producing high-quality cutin suitable for sustainable biomaterial applications.

## 2. Materials and methods

Several techniques were employed in this work and they are described in this section.

Fig. 1 summarizes the employed procedures to facilitate their understanding and what they were used for.
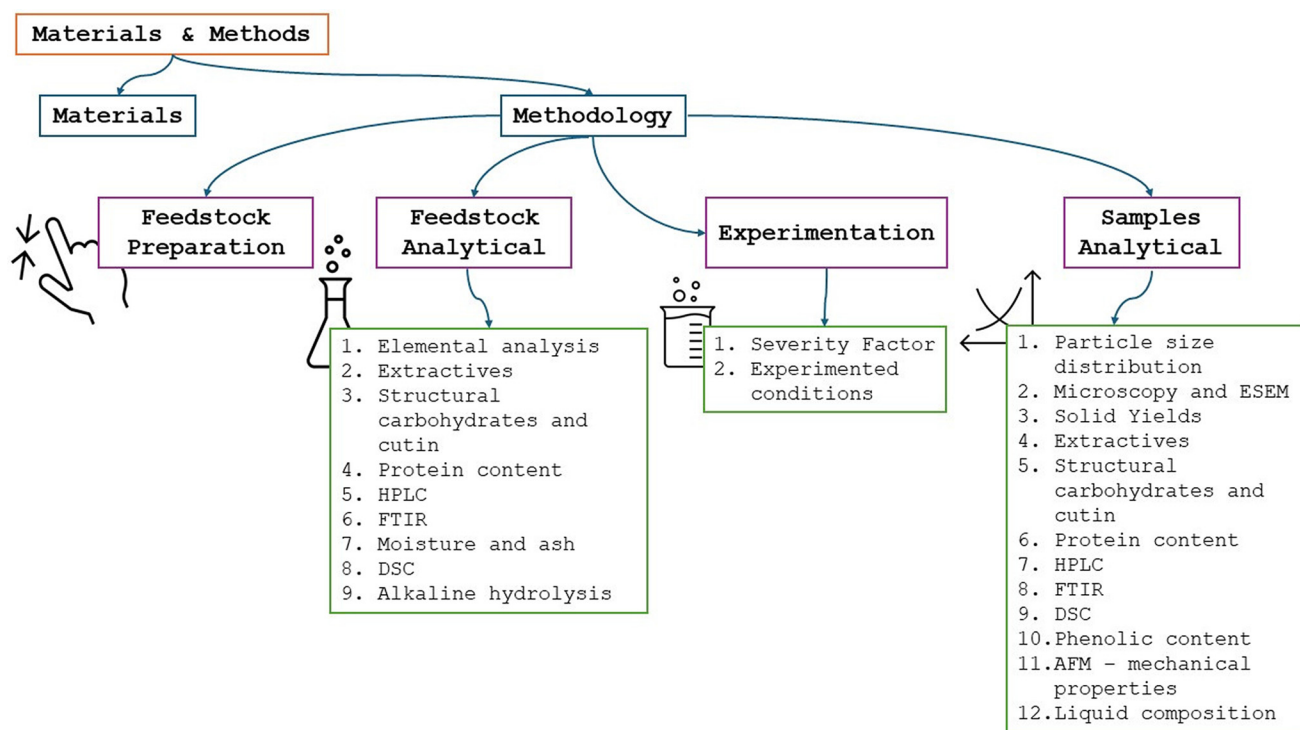
Fig. 1 Experimental and Analytical procedures.

### 2.1. Materials

Tomato pomace was provided by Pronat Company (Don Benito, Badajoz, Spain), with a processing capacity of 5600 tons per day, 300 000 tons of tomatoes per campaign.[30] The peel alone typically constitutes about 3% to 7% of the total weight of raw tomatoes in the processing industry. Acetic acid 99.5% was purchased from Panreac. Chloroform 99% and methanol ≥99.8% for UV, IR, HPLC, and ACS, used for Soxhlet extraction were purchased from Acros Organics and Panreac respectively. For acid hydrolysis, sulfuric acid 72% (w/w) was used. The 72% was prepared in our laboratory using 96% sulfuric acid purchased from Panreac. Sodium hydroxide pellets 98% and hydrochloric acid 37% w/w solution used for conventional way of cutin isolation were purchased from Panreac. Calcium carbonate >95% used for the neutralization of samples was purchased from Sigma Aldrich. Water used for Soxhlet extraction, experiments, and other analysis, when it was necessary, was Milli-Q and type III grade, produced in our laboratory, on equipment from company Millipore (Milan, Italy). Tomato peel cuticle obtained by enzymatic hydrolysis, as described in España *et al.*,[31] was obtained from the Department of Molecular Biology and Biochemistry, Faculty of Sciences, Teatinos Campus University of Malaga. The following components were used for preparation of standard calibration curves: glucose 99.5%, cellobiose 98%, fructose 99%, arabinose 99%, xylose 99%, glyceraldehyde 90%, glycolaldehyde dimer 100%, formaldehyde 36.5%, dihydroxyacetone 97%, hydroxyacetone 90% from Sigma Aldrich and formic acid 85% and acetic acid 99.8% from Panreac.

### 2.2. Methodology

**2.2.1. Tomato pomace separation – feedstock preparation.** To separate the peels and seeds fractions, around 1 kg of pomace was placed in approximately 5 l of type III water in the square-shaped container, well mixed. Then, the mix was left to settle for approximately 10 min, during which the fractions were separated. Seeds sedimented to the bottom of the container while the peels floated on the surface. Afterward, the peels were collected from the surface with a strainer. Some seeds remained in the peel fraction as this separation was not perfect. The absorbed water was first drained by squeezing and finally, the tomato peel fraction was placed in a ventilated room for approximately two weeks or in the oven with convection at 60 °C for 2 days for drying. Dry tomato peel contained approximately 5% w/w of moisture. Dry tomato peels were ground first in a kitchen blender and finally, ball milled using Retsch equipment, for 16 minutes milling time.

**2.2.2. Characterization of tomato peel.** Characterization of the tomato peel fraction was done to determine the structural composition of the received tomato peel used in future experiments. For this reason, several analytical methods were used, which are briefly described below.

*2.2.2.1. Elementary analysis.* The elemental composition of the tomato peels was determined at the Sciences and Technology Park, University of Burgos using EA Flash 2000 Elemental Analyzer (Thermo Fisher Scientific), TCD Detector, and Mettler Toledo XP6 Microbalance. The technique used for analysis was elemental analysis by combustion, where both organic and inorganic substances are converted into elemental

gases which, after subsequent reduction, are separated in a chromatographic column and transferred to a thermal conductivity detector.

*2.2.2.2. Soxhlet extraction.* The waxes and other unbounded compounds together were called extractives. Those were extracted by Soxhlet extraction with chloroform and methanol for 5 h separately and finally water extraction for 24 h. First, a rotary evaporator was used to evaporate solvents for chloroform and methanol extractives. Finally, extractives were placed in the oven at 50 °C overnight to dry completely. Water extractives were first frozen and afterward placed in a laboratory freeze dryer for a few days to dry completely. The total amount of extractives was calculated as the sum of individual fractions.

*2.2.2.3. Structural carbohydrates and cutin.* To determine the amount of carbohydrates in the extract-free tomato peel, acid hydrolysis was performed in two steps following the NREL procedure for the Determination of structural Carbohydrates and Lignin in Biomass[32] with some small changes in procedure. Briefly, extract-free samples were placed in pressure tubes and first treated with 72% sulfuric acid at 30 °C. Upon completion of 60 minute hydrolysis, the mixture was diluted so the acid reached a 4% concentration by adding deionized water, and tubes were then placed for 1 h at 120 °C. Afterward, the hydrolysis solution was cooled at room temperature and filtered through previously measured ashless filter paper. The solid phase on filter paper was washed several times with deionized water and placed in the oven at 40 °C overnight for drying while the liquid phase was neutralized with calcium carbonate up to pH 6 to prepare samples for HPLC sugar analysis.

Oven-dried solids on filter paper were measured and afterward placed in crucibles at 550 °C to determine ash. Oven-dry solids were considered cutin, which can be confirmed by FTIR analysis of this solid.

*2.2.2.4. Protein content.* Total Kjeldahl nitrogen was determined according to APHA Standards Methods and then total proteins were calculated as Kjeldahl N × 6.25. This technique allowed the determination of the protein content of the peel fraction, due to the remaining content of seeds, rich in protein.

*2.2.2.5. High performance liquid chromatography analysis.* For HPLC analysis of the aqueous products, a Shodex SH-1011 column at 50 °C was used. Sulfuric acid (0.01 N) was used as the mobile phase with a 0.8 mL min$^{-1}$ flow rate. A Waters IR detector 2414 was used to identify the sugars and their derivatives. Quantification was carried out using standard calibration curves.

*2.2.2.6. Fourier-transform infrared (FTIR) spectroscopy analysis.* To follow the structural changes in tomato peel before and after supercritical water hydrolysis SCWH and after conventional alkaline hydrolysis, Bruker Tensor 27 was used. All spectra were recorded in the range from 4000 to 400 cm$^{-1}$ with 4 cm$^{-1}$ resolution. The recorded spectra were baseline-subtracted and normalized to the maximum peak intensity.

*2.2.2.7. Determination of moisture and ash content.* The amount of moisture was determined following the NREL procedure for the Determination of Total solids in biomass and total dissolved solids in liquid process samples at 105 °C overnight while ash content was determined following the NREL procedure for the Determination of ash in biomass at 550 °C for at least 24 h.[33,34] The moisture amount was used for the calculation of oven dry weight (ODW). This value was later used for all calculations where ODW was required.

*2.2.2.8. Differential scanning calorimetry analysis.* Differential scanning calorimetry analysis (DSC) of raw tomato peel, the solid precipitate obtained after alkaline hydrolysis, and some solid parts of the products. The procedure was done as discussed in the reference.[12] The used device was a Mettler Toledo DSC 3+.

*2.2.2.9. Alkaline hydrolysis.* Alkaline hydrolysis of tomato peel for cutin isolation was performed as a conventional method with which the results of the method tested in this work were compared.[12] The tomato peel sample, which was previously exposed to above explained exhaustive Soxhlet extraction, is treated with 1M sodium hydroxide for 24 h at 100 °C. After this treatment, the sample is cooled down to room temperature and after that filtered through filter paper. The collected liquid is acidified with 3M hydrochloric acid to pH ~3. The precipitate is separated by centrifugation, washed with water several times, and dried using a freeze-dryer. The above-explained FTIR and DSC analysis were later used to study the dry precipitate.

**2.2.3. Experimental setup.** The experiments were done at two different devices that both, operate continuous Supercritical Water Hydrolysis (SCWH), named PHUn1 and PHUn2. The main difference between the two devices is that PHUn2 is an automated unit where pressure and temperature are controlled by a PLC. This control is manual in PHUn1. In addition, PHUn2 is a pilot scale plant with a maximum product suspension flow of 40 kg h$^{-1}$. The basic flow diagram, operating details, and procedure are given in a previous publication from our research group.[17,22,35]

*2.2.3.1. Severity factor: reaction time at 375 °C.* The severity factor ($D_0$) is commonly used in hydrothermal processes to quantify experimental conditions by combining the effect of reaction time ($t_i$) and temperature ($T_i$) into a single parameter representing the extent of the reaction. This is measured in time (seconds) at a reference temperature ($T_b$). This approach allows for the comparison of different reaction conditions on a common basis. Essentially, the severity factor adjusts the actual reaction time by accounting for the difference between the actual reaction temperature and a reference temperature. Reactions with similar $D_0$ are expected to have a similar extent of reaction, leading to comparable effects under different experimental conditions.[36] In this study, the reference temperature ($T_b$) was set to 375 °C (648.15 K) and $D_0$ was calculated using eqn (1). The calculated $D_0$ values are presented in Table 2.

$$D_0 = t_i \times \exp\left(\frac{T_i - T_b}{\omega}\right) \quad (1)$$

where $t_i$ is the reaction time (s), $T_i$ is the reaction temperature (K), and $T_b$ is the base or reference temperature (K). In most

**Table 2** Condition tested in experiments

| Equipment | No. | Reaction time | Reaction time at 375 °C | Average reaction temperature at steady state | Average reaction pressure at steady state |
|---|---|---|---|---|---|
| *PHUn1* | 1 | 0.25 s | 0.48 s | 390 ± 6 °C | 258 ± 7 bar |
| | 2 | 1.05 s | 1.84 s | 388 ± 2 °C | 254 ± 7 bar |
| | 3 | 6.33 s | 0.40 s | 312 ± 9 °C | 206 ± 8 bar |
| *PHUn2* | 4 | 0.06 s | 0.16 s | 398 ± 21 °C | 251 ± 1 bar |
| | 5 | 0.37 s | 0.86 s | 394 ± 4 °C | 251 ± 4 bar |
| | 6[a] | 0.49 s | 0.79 s | 386 ± 9 °C | 251 ± 3 bar |
| | 7 | 0.51 s | 0.80 s | 385 ± 11 °C | 251 ± 1 bar |
| | 8[a] | 0.52 s | 0.70 s | 382 ± 6 °C | 241 ± 1 bar |
| | 9 | 0.53 s | 0.70 s | 381 ± 8 °C | 241 ± 1 bar |
| | 10 | 0.89 s | 1.51 s | 387 ± 6 °C | 251 ± 1 bar |

[a] In those conditions acetic acid was added to the tomato peel suspension.

studies, the reference temperature is assigned to 100 °C. However, since the experiments were conducted near the critical point of water, where the reaction medium exhibits significantly different properties compared to those at 100 °C, 375 °C (648 K) was selected as the reference temperature. Further, $\omega$ is a fitted parameter (eqn (2)) where $T_f$ represents the middle of the range for experimental conditions (floor temperature) (K), $R$ is the universal gas constant (8.314 J (mol K)$^{-1}$) and $E_a$ is the activation energy of the biomass hydrolysis reaction (kJ mol$^{-1}$). In literature, a commonly used value for $\omega$ is 14.75 K, corresponding to the activation energy ($E_a$) of hemicellulose hydrolysis (111 kJ mol$^{-1}$). Applying this value to our system would be an oversimplification due to the complex composition of tomato peel biomass. Therefore, the activation energy of biomass was calculated as the weighted average of the activation energies of the tomato peel compounds (eqn (3)): cellulose (164 kJ mol$^{-1}$), hemicellulose (111 kJ mol$^{-1}$), and part of tomato peel which is calculated as pectin (111 kJ mol$^{-1}$). Additionally, the activation energy of protein (157 kJ mol$^{-1}$) is also considered although proteins are not originally part of the peel but seeds that remain in the peel fraction after the above-explained separation process.[36] These compounds of the tomato peel were chosen because they are expected to be primarily hydrolyzed in the process. For the $T_f$, the middle of experimental conditions was used at 350 °C. Taking this into account, the final number obtained for the activation energy was 141.11 kJ mol$^{-1}$ and the fitting parameter was 22.88 K.

$$\omega = \frac{T_f^2 R}{E_a} \quad (2)$$

$$E_a(\text{tomato peel}) = \sum (y_i \times E_{a\,i}) \quad (3)$$

*2.2.3.2. Experimental conditions.* The tested conditions are shown in Table 2. The raw material for these experiments was prepared by mixing milled raw tomato peel with deionized water in a way that the final concentration of suspension was between 4 and 11%. Additionally, experiments 6 and 8 (Table 2 below) were done with the addition of acetic acid in biomass suspension. This organic acid was added to drop the pH and promote the hydrolysis of polysaccharides (cellulose, hemicellulose, and pectin). The amount of added acetic acid was 50% on a dry basis suspension, which dropped the pH down to 2–3.

**2.2.4. Feed and product analysis.** For all performed experiments (see Table 2) sampling was done from two sources: prepared tomato peel suspension (hereafter called feed) and the sample obtained after the process (hereafter called product). Both feed and product, are a combination of suspended and dissolved solids in water. The liquid and solid phases were separated by centrifugation. The solid phase, after separation, was washed several times with water and left to dry.

*2.2.4.1. Particle size analysis.* The particle size of the feed and product was analyzed before centrifugation. The measurement was done by a Dynamic Light Scattering (DLS) Mastersizer 2000. The particle size distribution was calculated based on volume distribution.

*2.2.4.2. Microscopy and environmental scanning electron microscopy analysis.* The conventional microscopy method was used to study the surface morphology of raw tomato peel before and after the milling process (tomato peel in powder). The microscope-type Leica DM1000 LED from Leica Microsystems, Spain was used. Micrographs were obtained at 40× magnification.

An environmental scanning electron microscopy (ESEM) (FEI QUANTA 200 FEG ESEM, FEI Company Czech Republic) was used to study tomato peel powder and the product's surface characteristics. The product suspensions were analyzed, as obtained during the process, under low-vacuum conditions (0.6 mbar). Micrographs were obtained at 4000×, 5000×, and 80 000× magnification. Energy Dispersive Spectroscopy (EDS) data were collected with an EDAX Genesis module coupled to the ESEM.

*2.2.4.3. Characterization of the solid phase.* The solid yield was calculated following the coming procedures and equations. First, the total solids (TS), dissolved solids – water soluble material – (DS), and suspended solids – water insoluble material – (SS) was determined. Furthermore, the TS value is a direct measure of feed and product concentration. For TS analysis, approximately 2 g of well-mixed, homogeneous suspension was placed in a previously weighted aluminum pan and put in the oven at 105 °C overnight to dry. In the same way, DS was determined by filtering approximately

2 g of well-mixed, homogeneous suspension through a 0.22 μm filter in the previous weighted aluminum pan and putting it in the oven at 105 °C overnight to dry. Further, the SS value is obtained as the difference between TS and DS. Finally, the yield of the solid was calculated by eqn (4).

$$\text{Solid yield \%} = \frac{\dfrac{SS_{product}}{TS_{product}}}{\dfrac{SS_{feed}}{TS_{feed}}} \times 100\% \qquad (4)$$

The solid phase of feed and product was characterized by following the same procedure explained previously for the preliminary characterization of tomato peel fraction (see subtitles 2.2.2.2–2.2.2.9).

For the solid part of the products, the total phenolic content was determined as a sum of phenolic compounds that can be extracted by organic solvents such as methanol, and phenolic compounds remain inside the cutin matrix and can be released after the cutin structure is completely hydrolyzed by above explained alkaline hydrolysis. For the first part, the solid part of the product was subjected to extraction with methanol in the ratio of 1 : 10 (g : ml) at room temperature for one hour with constant stirring. Afterwards, the mixture was filtered by vacuum filtration to obtain liquid extract. For the phenolic compounds remaining inside the cutin matrix, the above-explained procedure for alkaline hydrolysis was performed on the solid part of the product which was previously exposed to soxhlet extraction. Phenolic compounds were determined from the liquid part obtained after the acidification step when fatty acids were precipitated. Finally, the concentration of phenolic compounds was determined by utilization of the Folin–Ciocalteu method on the UV-VIS spectrophotometer Shimadzu UV-2550.

In addition, in order to determine the mechanical properties and primarily Young's modulus of the obtained product, atomic force microscopy (AFM) analysis was performed on the solid part of the products rich in cutin. A dry solid part of the products, which was previously exposed to above explained exhausted Soxhlet extraction, was dispersed in tetrahydrofuran at a ratio of 1 : 9 and 10 μl of dispersion was drop cast on mica. The measurements were carried out in a Cypher ES AFM from Asylum Research (Oxford Instruments Asylum Research) following the procedure described by.[37,38] The data were acquired using a standard AC160TS cantilever from Olympus with a spring constant $k$ of approximately 26 N m$^{-1}$, a $Q$ factor of 289, and a resonant frequency of 269.7 kHz, 1.566 MHz. It used AM–FM mode, where it is possible to combine the information from the excitation of two cantilever resonances simultaneously, presenting a drive amplitude of 13.10 mV and 28.39 mV. In brief, the first resonance, in standard tapping mode (AM mode), allows topography to be determined through the first resonance amplitude. A second resonance, where the frequency was tracked by the controller (FM mode), allowed us to map both the conservative and dissipative components of the tip–sample interaction. This bimodal mode provides a simultaneous data topography and the local elastic modulus. The images were rendered and post-processed using the IGOR PRO software. The vales were fitted with Gaussian, providing both the mean and SD for each sample.

*2.2.4.4. Liquid phase analysis.* The liquid part of the samples was analyzed to determine the yield of products of hydrolysis of polysaccharides after SCWH, primarily C5 (hemi-cellulose derived) and C6 (cellulose derived) sugars as well as sugar degradation products. To transform the product oligomers in the liquid phase into monomeric sugars that can be detected and measured by HPLC, the liquid phase of the samples was subjected to one-step acid hydrolysis. The procedure involved adding 72% w/w sulfuric acid to the product sample in a way that the final acid concentration was 4% w/w. Hydrolysis was run for 1 h at 120 °C. Finally, the sample was cooled at room temperature and neutralized with CaCO$_3$ up to pH 6 to prepare it for HPLC analysis. Thereafter, HPLC analysis was done by the method described in section 2.2.3.4.

# 3. Results and discussion

This section presents the findings on extracting and enriching native cutin from tomato peel waste using sudden supercritical water hydrolysis (SCWH). Detailed are the compositional analysis, particle size distribution, and structural characterization of the solid and liquid products.

### 3.1. Tomato peel elementary analysis and characterization

The elemental composition of the tomato peel used in this study is presented in Table 3. Carbon was the predominant element, consistent with the organic nature of biomass. A nitrogen content of 1.5% indicates the presence of proteins, likely originating from residual tomato seeds remaining with the peel after separation.

The composition analysis of the tomato peel fraction is detailed in Table 4. Cutin constitutes approximately 52.9% of the dry weight, confirming it as the main component. These findings align with previous reports,[39,40] validating the use of tomato peel as a viable source for cutin production.

**Table 3** Elementary composition

| Element | N | C | H | S |
|---|---|---|---|---|
| Amount, % | 1.5 ± 0.1 | 58.8 ± 0.1 | 8.3 ± 0.1 | 0.00 |

**Table 4** Compositional analysis for tomato peel (dry basis)

| Fraction | Amount, % w/w |
|---|---|
| Extractives | 13.2 ± 2.0 |
| Cutin | 52.9 ± 1.7 |
| Cellulose | 11.0 ± 3.3 |
| Hemicellulose | 2.6 ± 0.4 |
| Protein | 9.7 ± 0.6 |
| Ash | 1.6 ± 0.1 |
| Others | 9.0 |

### 3.2. Particle size analysis

Particle size distribution refers to the range of particle sizes present in a material sample. Analyzing particle size distribution can provide valuable information across various fields including materials science, pharmaceuticals, environmental science, and manufacturing.[41] Therefore, this analysis was carried out for all products obtained after the SCWH as well as for the feed suspension. Fig. 2 illustrates the normal distribution of particle size for both feed (right) and products (left). The ESI Table S1 (ESI†) shows the values of $d(0.1)$, $d(0.5)$, and $d(0.9)$ for each sample. The feed particle sizes were primarily influenced by ball milling efficiency. Minor deviations were observed despite consistent milling conditions, with some samples exhibiting bimodal distributions, with the main peak around 100 μm and the secondary around 40 μm and 20 μm respectively. Most of the feed particles were below 250 μm in diameter.

On the other side, the products displayed a significant reduction in particle size, approximately one order of magnitude smaller than the feedstock. This shift indicates the effectiveness of SCWH in breaking down the biomass structure. Notably, the products from experiments with reaction times of 1.84 s and 1.51 s (see Table 2) shows unimodal distribution. Interestingly, these two experiments also had the most severe conditions among the experiments done on PHUn1 and PHUn2, and they underwent the biggest changes compared to the initial composition of the feed which is explained more in the other analysis below. Although these two experiments show a more uniform unimodal distribution, the peak is located at larger values. This observation is likely related to the composition of the solids. Higher severity meant higher hydrolysis of cellulose, hemicellulose, and pectin, which can be associated with the smaller particle size in the distribution.

### 3.3. Process performance

The main objective of this work was to extract cutin from tomato peel while preserving its native three-dimensional polyester network. Since cutin is chemically stable, it was expected to remain in the solid phase post-hydrolysis. Hence, close attention was paid to the characterization of the solid phase of the products (SS). The experimental conditions (see Table 2) were designed to selectively hydrolyze other tomato peel constituents like cellulose, hemicellulose, and protein.

The solids yields, calculated using eqn (4), are presented in Fig. 3. The results are separated according to the device used for the experiment. High solid yield were observed across all experiments due to the high content of water-insoluble components like cutin and waxes. However, a decreasing trend in solid yield was noted with increasing severity of reaction conditions, (Fig. 3A and B). For instance, at mild severity of 0.16 s, 94.3% w/w of the suspended solids that entered the reactor remained as solid after the hydrolysis (Fig. 3B). Almost the same was observed on PHUn1 for conditions of 0.40 s and 0.48 s, yields were 92.2% w/w and 92.1%, respectively (Fig. 3A). Also, it should be noted that the experiment with a condition of 0.40 s was the only experiment done in water subcritical conditions, at the reaction temperature of 312 °C and, therefore, the experiment was conducted with a significantly longer actual reaction time of 6.3 s (see Table 2). On the other side, more severe conditions (1.51 s on PHUn2 and 1.84 s on PHUn1) resulted in reduced yields of 70.1% and 83.8%, respectively. Finally, the addition of acetic acid did not significantly impact the solid yield (Fig. 3C).

The compositions of the solid products are shown in Fig. 4. The composition of the tomato peel can be variable for different batches. Therefore, to achieve a correct mass balance, the results were compared with the characterization of each solid feed. Additionally, in the ESI Table S2 (ESI†), the mass balance for samples and feed is presented. Post-hydrolysis, there was an increase in cutin and extractives content, while cellulose, hemicellulose, and protein contents decreased due to their hydrolysis and solubilization. Hemicellulose was completely hydrolyzed under all conditions, indicating its high lability.

The proportion of cellulose and protein remaining in the solid products (see Fig. 5) was calculated using eqn (5), where "$y_{i\,product}$" is the mass fraction of component '$i$' in the suspended solids of the product, and "$y_{i\,feed}$" is the mass fraction of component '$i$' in the suspended solids of the feed, SS$_{product}$,
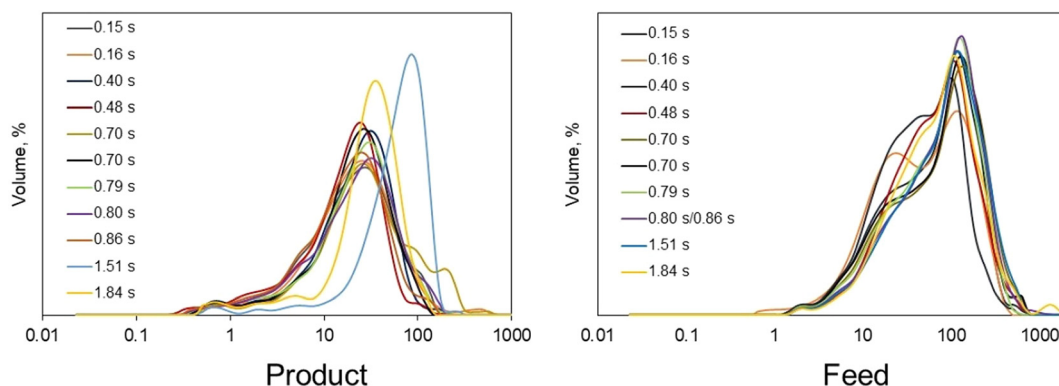


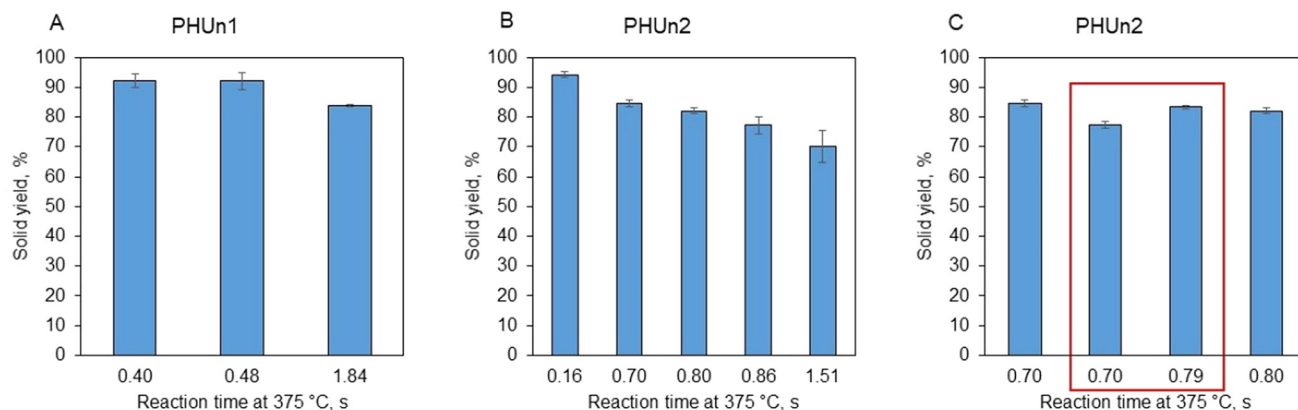**Fig. 2** Normal distribution of particles in the size of products and feeds.

**Fig. 3** Solid yield for experiments done on PHUn1 (A), on PHUn2 (B) and comparison of solid yields for experiments without and with the addition of acetic acid − framed (C).
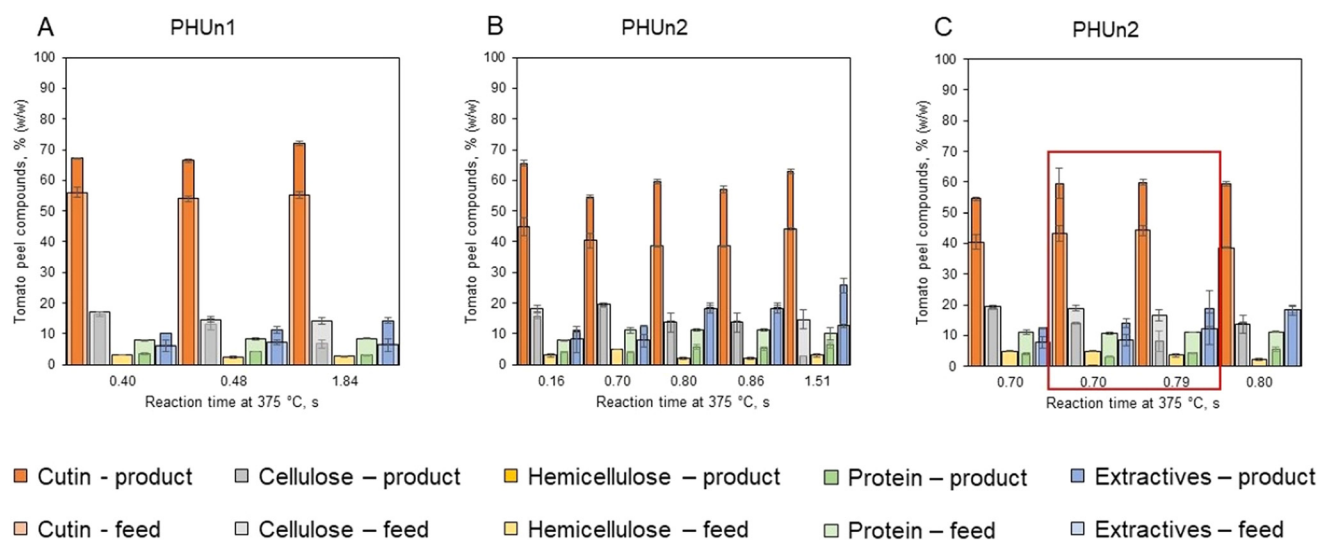


**Fig. 4** Solid product composition and feed composition over different reaction times at 375 °C for experiments done on PhUN1 (A), on PhUN2 (B) and comparison of experiments without and with the addition of acetic acid − framed (C).
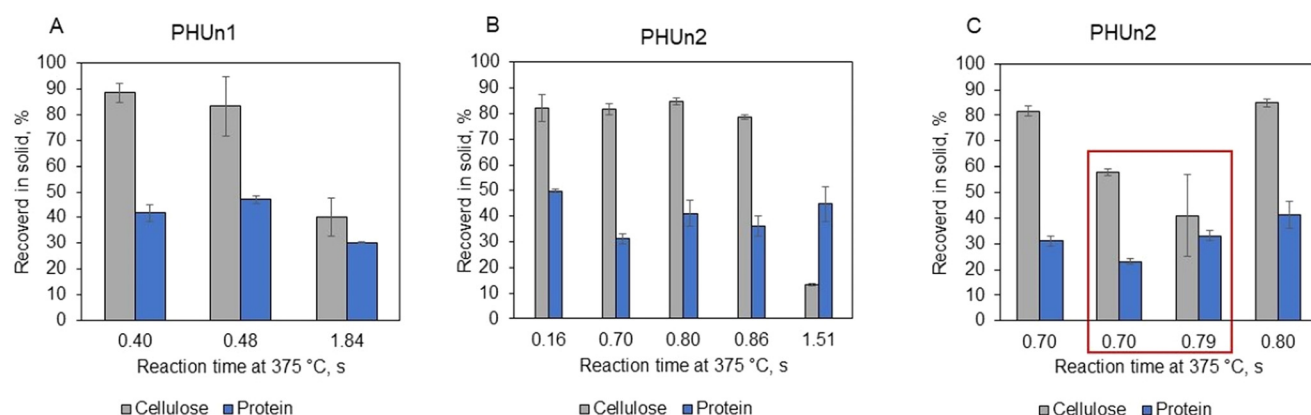


**Fig. 5** The amount of cellulose and protein remaining in the solid part of the product after the process for experiments done on PhUN1 (A), on PhUN2 (B) and comparison of experiments without and with the addition of acetic acid − framed (C).

$TS_{product}$, $SS_{feed}$, and $TS_{feed}$ were explained before. Cellulose showed significant resistance to hydrolysis, with 80 to 90% remaining unhydrolyzed under mild conditions. Still, it should be noted that those results were obtained with less than 1 second of reaction time. A more significant change happened at more severe conditions of 1.84 s in PHUn1 and 1.51 s in PHUn2 when the solid part of products contained 6.8% and 2.8% of the cellulose, which represents 40% and 13% of cellulose in feed, respectively. This amount of cellulose in the solid products was higher compared to other biomasses previously tested by our group. For instance, only 1% of the cellulose was recovered as a solid product under similar conditions when hydrolyzing sugar beet pulp.[22] Another point of comparison is the high-lignin materials, like grape seeds. The hydrolysis of these materials reported values of cellulose recovery of less than 10% at similar conditions to this work. These feedstocks have a complex structure where lignin acts as a barrier to hydrolysis of polysaccharides.[20] Although the tomato peel structure is not as complex as the lignocellulose structure in grape seeds, the recalcitrance of cellulose can be attributed to strong hydrogen bonds formed between water molecules, cutin and cellulose.[6] The addition of acetic acid enhanced cellulose hydrolysis, reducing the unhydrolyzed fraction from 81.6% to 57.8% for the reaction condition of 0.70 s, and from 84.8% to 41.0% for the reaction condition of 0.80 s. Finally, regarding protein content in the solid products, between 30% and 50% of protein remained unhydrolyzed for all conditions. The addition of acetic acid had some impact on protein hydrolysis. Accordingly, the amount of unhydrolyzed protein decreased from 31.1% to 23.0% when acetic acid was added for the reaction condition of 0.70 s and from 41.1% to 33.1% for the reaction condition of 0.80 s.

$$\text{Recovery of } i, (\%) = \frac{y_{i\,\text{product}} \times \dfrac{SS_{product}}{TS_{product}}}{y_{i\,\text{feed}} \times \dfrac{SS_{feed}}{TS_{feed}}} \times 100 \quad (5)$$

Phenolic compounds were analyzed due to their influence on the mechanical properties of the cutin matrix. The phenolic compounds contribute to the rigidity of the cutin matrix and it is the highest at full maturity of tomato fruit.[31] Table 5 shows the results for total phenolic content of two products obtained in the process at less severe conditions (0.48 s) and more severe conditions (1.51 s). The amount of phenolic compounds extracted by methanol was slightly higher at more severe conditions. Applying more severe conditions resulted in higher hydrolysis and removal of tomato peel components. Then it

could be speculated that this product offers less mass transfer barrier, which results in higher efficiency of the methanol extraction process. Interestingly, slightly lower percentages were obtained for the Soxhlet extraction method. The obtained amount was 1.69% ± 0.48% for less severe conditions (0.48 s) and 1.53% ± 0.04% for more severe conditions (1.51 s). However, the Soxhlet extraction with methanol was done after extraction with chloroform, where some amount of phenolic was likely removed. On the other hand, the phenolic compounds inside the cutin matrix was significantly higher at less severe conditions. Such results are in correlation with the previous considering that at less severe conditions, the preservation of the cutin matrix is higher.

### 3.4. FTIR analysis

The Fourier Transform Infrared (FTIR) spectra of various samples – including raw tomato peel, extract-free tomato peel after acid hydrolysis (ext-free TP – acid hydrolysis), extract-free tomato peel after alkaline hydrolysis (ext-free TP – alkaline hydrolysis), cutin obtained after acid hydrolysis of dewaxed tomato peel cuticle following the procedure described in España et al.[31] (reference cutin) and products obtained after sudden supercritical water hydrolysis (SCWH) at low severity (0.48 s) and high severity (1.51 s) are presented in Fig. 6. The main absorption bands and their assignment are listed in Table 6, indicating the corresponding components within the tomato peel.

**3.4.1. Wavenumber range 2800–3700 cm⁻¹.** Fig. 6A focuses on the spectra within the wavenumber range of $2800\ \text{cm}^{-1}$–$3700\ \text{cm}^{-1}$. An intense band at approximately $3337\ \text{cm}^{-1}$, associated with O–H stretching vibrations, is observed in the raw tomato peel. This band's intensity decreases significantly in the spectra of the acid-hydrolyzed sample, alkaline-hydrolyzed sample, and SCWH products. The majority of O–H groups in tomato peel originate from cutin and polysaccharides.[42] The reduction in the O–H band intensity indicates the removal of polysaccharides during acid hydrolysis, alkaline hydrolysis, and the SCWH process. Dominant bands at $2923\ \text{cm}^{-1}$ (asymmetric stretching of a methylene groups) and $2852\ \text{cm}^{-1}$ (symmetric stretching of a methylene group) are attributed to the long-chain aliphatic groups present in cutin and waxes. These bands are consistently observed across all samples, suggesting that the aliphatic components remain largely unaffected by the treatments.

**3.4.2. Wavenumber range 700–1800 cm⁻¹.** Fig. 6B displays the spectra within the wavenumber range $700\ \text{cm}^{-1}$–$1800\ \text{cm}^{-1}$. Characteristic ester bond vibrations are identified by three high-intensity bands at $1728\ \text{cm}^{-1}$ (C=O stretching), $1163\ \text{cm}^{-1}$ (asymmetric C–O–C stretching), and $1102\ \text{cm}^{-1}$ (symmetric C–O–C stretching). These bands are present in the spectra of raw tomato peel, extract-free TP–acid hydrolysis, and SCWH products (0.48 s and 1.51 s). The only sample showing different band behavior at this wavelength is the ext-free TP – alkaline hydrolysis. The persistence of these bands in the SCWH products indicates that the ester bonds in cutin remain intact after the hydrolysis process, suggesting that the native
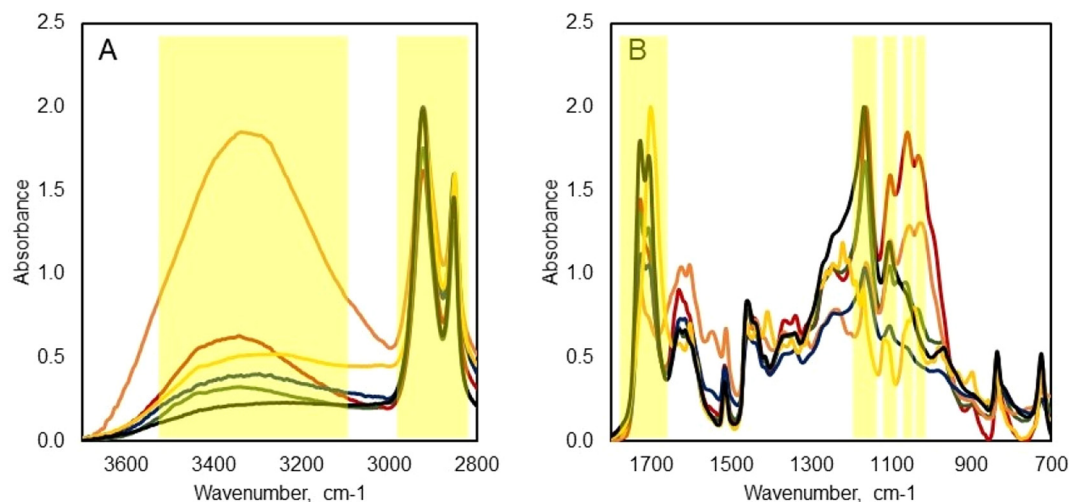
**Table 5** The content of phenolic compounds in the products

| Product | Phenolic compounds – methanol, % | Phenolic compounds inside cutin matrix, % | Total phenolic compounds, % |
|---|---|---|---|
| 0.48 s | 2.22 ± 0.03 | 3.17 ± 0.08 | 5.39 |
| 1.51 s | 2.85 ± 0.11 | 1.48 ± 0.07 | 4.33 |

**Fig. 6** FTIR spectrum of raw tomato peel (orange), ext free TP acid hydrolysis (blue), ext free TP alkaline hydrolysis (yellow), reference cutin (black), product 0.48 s (red), and product 1.51 s (green) in the range of wavenumber 2800–3700 cm$^{-1}$ (A) and 700–1800 cm$^{-1}$ (B).

**Table 6** The main FTIR peaks and their assignments

| Assignment | Product 0.48 s | Product 1.51 s | Raw tomato peel | Ext free TP – acid hydrolysis | Ext free TP – alkaline hydrolysis | Reference cutin | Tomato peel component |
|---|---|---|---|---|---|---|---|
| $\nu$(O–H⋯O) | 3344 | 3339 | 3337 | 3339 | 3339 | 3035 | Cutin, polysaccharides[42] |
| $\nu a$(CH$_2$) | 2923 | 2923 | 2921 | 2923 | 2923 | 2923 | Cutin, waxes[42] |
| $\nu s$(CH$_2$) | 2852 | 2852 | 2852 | 2852 | 2850 | 2852 | Cutin, waxes[42] |
| $\nu$(C=O) ester | 1728 | 1728 | 1728 | 1726 | — | 1728 | Cutin[42] |
| $\nu$(C=O⋯H) ester | — | 1710 | — | 1707 | — | 1707 | Cutin[42] |
| $\nu$(C=O⋯H) acid | — | — | — | — | 1701 | — | Cutin[42] |
| $\nu$(C=C) phenolic acid | 1632 | 1634 | 1626 | 1628 | 1630 | 1630 | Phenolic compounds[42] |
| $\nu$(C–C) aromatic | — | — | 1605 | — | 1603 | — | Phenolic compounds[42] |
| $\nu$(C–C) aromatic | 1557 | — | — | — | — | — | Phenolic compounds[42] |
| $\nu$(C–C) aromatic (conjugated with) | 1518 | 1516 | 1514 | 1516 | 1516 | 1518 | Phenolic compounds[42] |
| $\delta$(CH$_2$) scissoring | 1455 | 1461 | — | 1457 | 1463 | 1461 | Cutin, waxes[42] |
| $\nu$(C–C) aromatic (conjugated w) | — | — | 1438 | — | 1436 | — | Phenolic compounds[42] |
| $\delta$(CH$_2$) wagging and twisting | 1367 | 1365 | 1369 | — | 1371 | — | Cutin, waxes[42] |
| $\delta$(OH) | 1248 | 1246 | 1236 | 1242 | 1246 | — | Cutin, polysaccharides[42] |
| $\nu a$(C–O–C), ester | 1163 | 1167 | 1163 | 1167 | 1169 | 1169 | Cutin[42] |
| $\nu s$(C–O–C), ester | 1102 | 1104 | 1102 | 1104 | — | 1106 | Cutin[42] |
| $\nu$(C–O–C), glycosidic bond | 1059 | 1065 | 1055 | — | 1057 | — | Polysaccharides[42] |
| $\nu$(C–O) | — | — | — | 983 | 981 | 969 | Cutin, polysaccharides[42] |
| $\gamma$(C–H) aromatic | 834 | 834 | 832 | 832 | 836 | 834 | Phenolic compounds[42] |
| $\delta$(CH$_2$) rocking | 722 | 724 | 720 | 722 | 722 | 724 | Cutin, waxes[42] |

structure of cutin is preserved under the SCWH conditions employed (see Table 6).

On the other side, the ext-free TP-alkaline hydrolysis sample exhibits a different spectral profile. The bands at 1728 cm$^{-1}$ and 1102 cm$^{-1}$ are absent, and the band at 1169 cm$^{-1}$ is significantly diminished. A new intense band appears at 1701 cm$^{-1}$, associated with carboxylic acid (C=O⋯H) groups.[42] These observations confirm that during alkaline hydrolysis, ester bonds are cleaved, resulting in the destruction of the native ester structure of cutin.

The band at 1055 cm$^{-1}$, attributed to the stretching vibrations of glycosidic bonds and considered a fingerprint for polysaccharides,[43] is identified in the spectra of raw tomato peel and the SCWH products (0.48 s and 1.51 s).

Notably, the intensity of this band is significantly reduced in the spectrum of the 1.51 product compared to the raw tomato peel and 0.48 s product. This reduction indicates that polysaccharides are increasingly hydrolyzed under more severe SCWH conditions. This band is absent in the ext-free TP – acid hydrolysis spectrum, indicating that acid hydrolysis effectively removes polysaccharides from tomato peel. This band can be noticed in the spectrum of ext-free TP – alkaline hydrolysis at 1057 cm$^{-1}$, however, it is not as strong as in the spectrum of raw tomato peel and can relate to incomplete hydrolysis or contamination.

Several bands associated with phenolic compounds are observed at 1632 cm$^{-1}$, 1518 cm$^{-1}$, and 834 cm$^{-1}$ in the products obtained under both mild (0.48 s) and severe (1.51 s)

SCWH conditions. These bands correspond to C=C stretching vibrations in phenolic acids and aromatic C–H bending modes. While some phenolic can be removed during Soxhlet extraction, others remain trapped or chemically bonded to the cutin matrix. The presence of these phenolic bands in the SCWH products provides additional evidence that the complex structure of cutin, including its associated phenolic components, remains intact after the hydrolysis process.

When comparing the spectra of the extract-free TP–acid hydrolysis sample and the SCWH product obtained under more severe conditions (product 1.51 s) to the reference cutin sample (Fig. 6A and B), strong similarities become apparent. Notable observations include a significant reduction in the intensity of the peak corresponding to O–H stretching vibrations, the clear presence of peaks associated with ester bonds characteristic of cutin, and the absence (or, in the case of product 1.51 s, a drastic reduction) of peaks related to glycosidic bonds in polysaccharides. These findings confirm that the acid hydrolysis methodology employed in this study is an effective analytical tool for cutin quantification. More importantly, product 1.51 s, obtained through SCWH in an actual reaction time of less than 1 s, demonstrates exceptionally high purity, comparable to the reference cutin. The reference sample itself was derived from the chemical treatment of dewaxed cuticle after enzymatic treatment of tomato peel over a period of at least two weeks, highlighting the efficiency of the SCWH process. The FTIR analysis demonstrates that SCWH effectively preserves the native ester bonds and overall molecular structure of cutin in tomato peel. The minimal changes in key absorption bands associated with cutin, coupled with the reduction of bands corresponding to polysaccharides, indicate that non-cutin components are selectively hydrolyzed while the cutin network is maintained. These findings support the conclusion that SCWH is a suitable method for extracting cutin with its native three-dimensional structure preserved, making it a promising approach for producing bio-based materials.

The ability to continuously produce cutin of this quality within approximately one second raises important considerations regarding the scalability of this process. Notably, as mentioned above, a single industrial tomato processor in Spain processes approximately 300 000 tons per campaign, with 3–7% of this amount classified as waste. Currently, this waste has no applications, with only a small fraction being utilized as poultry feed. This suggests that for potential industrial implementation, the availability of raw materials would be relatively stable, which is a key factor in process feasibility.

From an energy perspective, there are multiple opportunities for optimizing energy efficiency. Several strategies are already being implemented in our laboratory, including utilizing the hot product stream to preheat incoming water and employing flash separators to concentrate the product. Further details on these energy-saving measures, as well as the broader implementation and sustainability of this technological approach, are discussed in the section 3.9.

### 3.5.  DSC analysis

Fig. 7 presents the Differential Scanning Calorimetry DSC thermograms for raw tomato peel, the solid precipitate obtained after alkaline hydrolysis (ext free TP alkaline hydrolysis), and the solid products obtained under less severe (0.48 s) and more severe (1.84 s) conditions. The DSC thermograms of the ext-free TP alkaline hydrolysis sample exhibits a distinct single melting peak at 57 °C, consistent with data reported in literature[12] for cutin monomers resulting from alkaline hydrolysis. On the other hand, the thermograms for raw tomato peel and the SCWH products show no observable melting transitions within the measured temperature range. The absence of melting peaks in the SCWH solid products indicates that the cutin remains in its native, cross-linked polymeric form rather than being hydrolyzed into monomeric units that would display melting behavior. This observation confirms that the SCWH process preserves the native three-dimensional polyester network of cutin, maintaining its structural integrity similar to that found in the original tomato peel.

### 3.6.  AFM analysis

Atomic Force Microscopy (AFM) analysis was performed on the solid fractions of two products of SCWH of tomato peel. The first product was obtained under mild conditions (reaction time of 0.48 s), resulting in a higher content of residual cellulose and other non-cutin components. The second product was obtained under more severe conditions (reaction time of 1.51 s), where a greater extent of hydrolysis of non-cutin components occurred. The results are presented in Table 7 and Fig. 8.
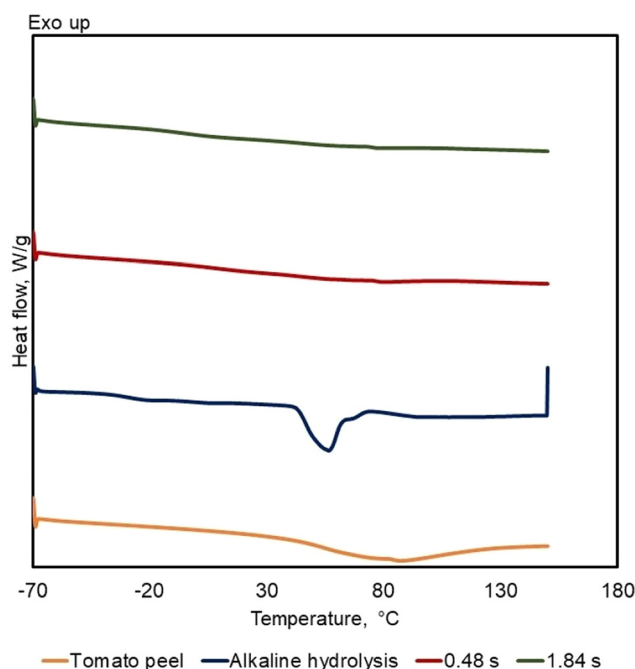


**Fig. 7** DSC of raw tomato peel, ext free TP alkaline hydrolysis, and two solid parts of products.

**Table 7** Young's modulus, phase and frequency of products

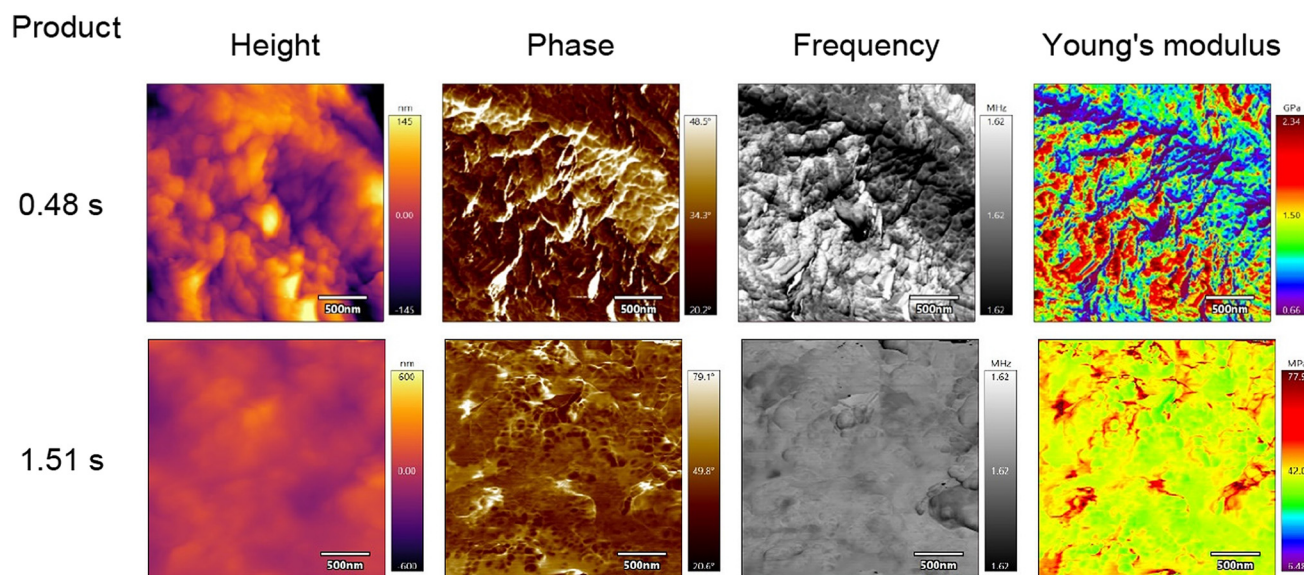| Product | Young's modulus, GPa | Phase, ° | Frequency (MHz) |
|---|---|---|---|
| 0.48 s | 1.3 ± 0.1 | 31.6 ± 2.5 | 1.6 ± 0.0 |
| 1.51 s | 0.7 ± 0.5 | 54.9 ± 10.3 | 1.6 ± 0.0 |

Plant tissues exhibit complex mechanical behavior that can be modified during growth or in response to external forces.[4] Factors influencing mechanical properties include polymer density, the presence of fillers and plasticizers in the polymer matrix, humidity, and temperature.[44] In the case of tomato peel, which has a complex structure dominated by polymers such as cutin and cellulose, mechanical properties are highly dependent on the development stage of the fruit. Although no significant mechanical differences are detected between the cuticles of immature and mature green tomatoes, ripening causes a notable increase in stiffness and a reduction in strain.[31] This effect is attributed to increased cross-linking of cutin and the accumulation of phenolic compounds within the cutin matrix during ripening.[45] Given the variability in mechanical properties due to these factors, direct comparison of Young's modulus values obtained in this study with those reported in the literature may be challenging. Furthermore, few studies have investigated the mechanical behavior of plant cutin using AFM. One such study highlighted the significant influence of moisture content on the mechanical properties of cutin, where an increase in humidity resulted in a substantial decrease in Young's modulus.[46] The Young's modulus values reported in the literature are considerably lower than those measured in the present study (see Table 7). The AFM analysis demonstrates that a higher residual cellulose content correlates with increased stiffness of the material, as indicated by a

higher Young's modulus. Cellulose is known to enhance structural rigidity due to its high tensile strength and stiffness. Moreover, the product obtained under milder conditions (0.48 s) exhibited a greater concentration of phenolic compounds embedded within the cutin matrix (refer to Table 5). The presence of phenolic compounds can contribute to increased rigidity of the cutin structure through additional cross-linking and interactions within the polymer matrix.

The AFM images presented in Fig. 8 reveal homogenous surfaces with well-defined features approximately 80–120 nm in size. The tested solid parts of products exhibited similar topography. The height images provide a direct representation of the surface morphology, while the phase images capture variations in phase shifts across the sample surface. These phase shifts result from differences in the sample's chemical composition or viscoelastic properties of the materials. Notably, the product obtained under more severe reaction conditions (1.51 s) exhibited a greater phase shift compared to the product from milder conditions. This observation suggests alterations in the material's viscoelastic properties, potentially due to the reduced content of non-cutin components and changes in the cutin network.

### 3.7. ESEM analysis

The surface morphology of raw tomato peel before milling showed the characteristic structure of epidermal cells, as shown in Fig. 9A. The cell sizes varied from 30 μm upwards. This type of structure has been previously reported in the literature.[47] After the milling process, which reduced the particle size to less than 250 μm (see Table S1 in the ESI†), the epidermal cell structure was disrupted, as evident in Fig. 9B. This observation was further confirmed by the ESEM image of the powdered tomato peel (Fig. 9C).



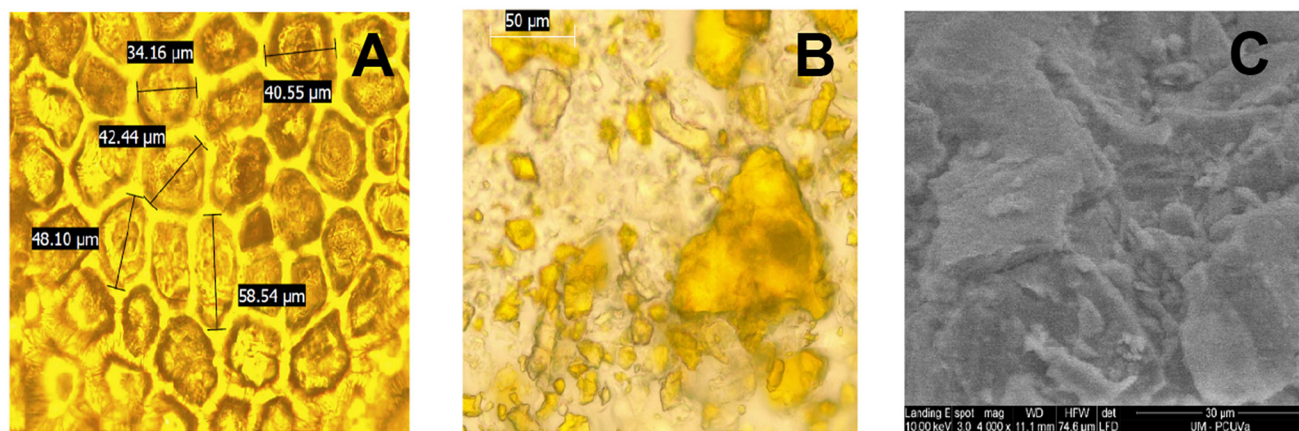**Fig. 8** Height, phase, frequency, and Young's modulus images obtained by AFM.

**Fig. 9** Microscope pictures of raw tomato peel before milling (A) and after milling (B) and ESEM picture of tomato peel after milling (C).

ESEM images of the products obtained after SCWH are presented in Fig. 10. These images were capture from product suspensions after the process to prevent coagulation or any other alterations on surface morphology during drying. A slight increase in roughness is noticeable when compared to the raw tomato peel (Fig. 9C); however, no significant differences in surface morphology were observed among the products, regardless of the reaction conditions applied. When compared to literature data of SEM images of cutin monomers used in film production with alginate, both before or after thermal treatment (polycondensation),[48] the surface morphology of the samples obtained thtough SCWH resembles that of polymerized samples, exhibiting a relatively smooth surface. Finally, this similarity suggests that, despite the drastic reduction in

particle size during the process, the main structural integrity of the material, with cutin as the dominant component, remained unaffected.[49]

### 3.8. Liquid phase analysis

The liquid portion of the products, collected after centrifugation, was analyzed to determine the concentrations of C5 and C6 sugars, as well as sugar degradation products. Yields were calculated using eqn (6). In this equation, $C_i$ represents the concentration of component '$i$' in the liquid product (where $i$ denotes C5 sugars, C6 sugars, or sugar degradation products), and $C_{cellulose}$, $C_{hemicellulose}$, and $C_{other}$ represent the concentration of cellulose, hemicellulose, and other components (primarily pectin) in the feed.
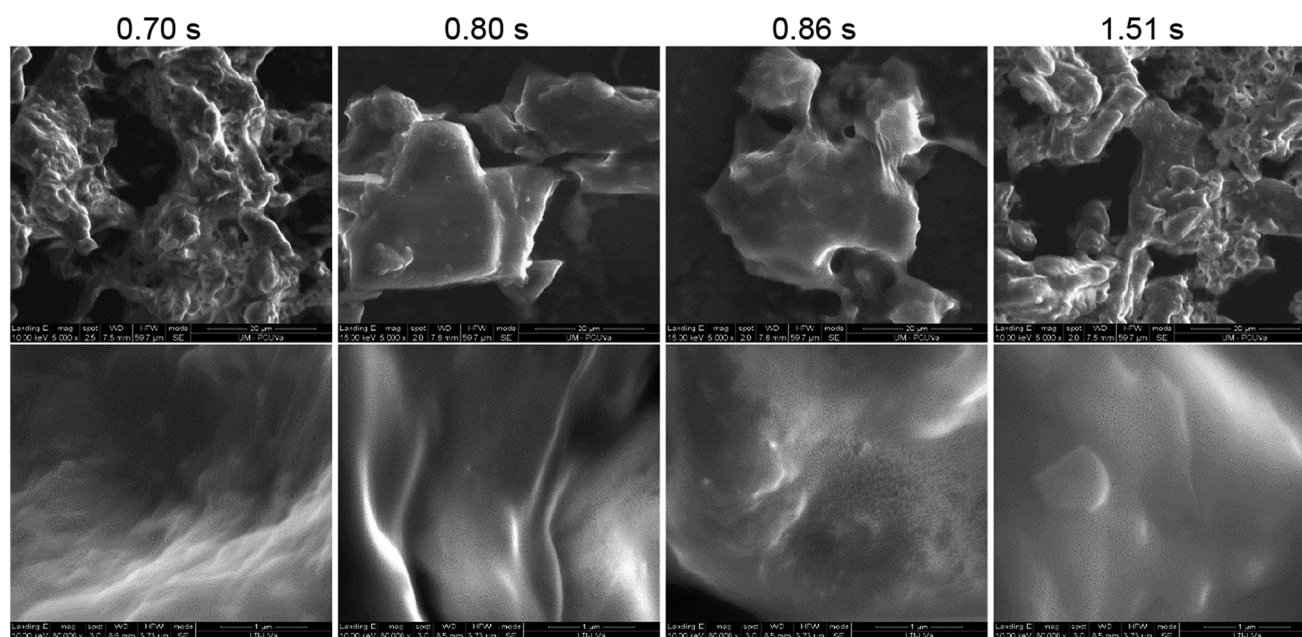


**Fig. 10** ESEM picture of product's suspensions for different applied conditions: upper row 5000× magnification; bottom row 80 000× magnification.

$$Y_i = \frac{\dfrac{C_{i\,\text{product}}}{\text{TS}_{\text{product}}}}{(C_{\text{cellulose}} + C_{\text{hemicellulose}} + C_{\text{other}})_{\text{feed}}} \times 100\% \qquad (6)$$

Xylose and arabinose were the C5 sugars detected in the liquid products. The highest yield of C5 sugars was achieved under reaction conditions of 0.48 s (actual reaction time of 0.25 s, see Table 2) in PHUn1 (Fig. 11A) and 0.86 s (actual reaction time of 0.37 s, see Table 2) in PNUn2 (Fig. 11B); beyond these conditions, the yields began to decrease. These results are similar to or slightly higher than those obtained in SCWH of grape seeds, where the maximum C5 sugar yield was reached at a reaction time of 0.27 s.[20] In contrast, for sugar beet pulp and wheat bran, shorter reaction times of 0.11 s, and 0.19 s, respectively, were necessary to achieve maximum yields.[22,50] In previous studies with grape seeds, sugar beet pulp, and wheat bran, the maximum yields of C6 sugars were obtained at the same reaction time as for C5 sugars. However, the behavior of C6 sugars yields from tomato peel differed significantly from that of C5 sugars. The yield of C6 sugars, which predominantly originate from cellulose and appear as glucose and cellobiose after SCWH of tomato peel, did not reach a maximum under the conditions tested. Instead, the yield increased slowly at first, with significant increases observed only under the most severe conditions (reaction time at 375 °C of 1.84 s on PHUn1 and 1.51 s on PHUn2, see Table 2). At these conditions, the yield of C6 sugars increased, but simultaneously, the yield of sugar degradation products also increased. These findings are consistent with the analysis of the solid products, which showed that a significant amount of cellulose was removed only under the most severe conditions. On the other hand, hemicellulose was the most labile component of tomato peel, undergoing hydrolysis more readily. Furthermore, as illustrated in Fig. 11C, the addition of acetic acid increased the yields of both C6 and C5 sugars. The most pronounce effect was observed for C6 sugars at a reaction time of 0.70 s, where the yield increased from 8.6% without acetic acid to 14.4% with acetic acid, and at 0.80 s, from 12.3% without acetic acid to 17.2% with acetic acid. This enhance-

ment is likely due to acetic acid's catalytic effect on the hydrolysis of cellulose and hemicellulose, facilitating the breakdown of these polymers into soluble sugars.

### 3.9. Discussion on process scalability and sustainability

Supercritical water hydrolysis (SCWH) offers distinct advantages for industrial-scale biopolymer recovery, largely because of its extremely short reaction times, often on the order of seconds. This rapid reaction rate drastically lowers the required reactor volume and simplifies reactor design (commonly tubular systems). Consequently, it facilitates straightforward scale-up from laboratory (TRL 4) and pilot (TRL 5) levels to a demonstration or commercial scale, minimizing both capital and operational costs. Indeed, Martínez et al.[22] have illustrated the successful scale-up of SCWH systems, highlighting this approach's capability to handle higher throughputs with only modest modifications to pumps, piping, and other supporting equipment.

From an industrial feasibility standpoint, Renmatix (USA)[51] operates SCWH technology at an industrial-demo scale, reinforcing scalability and commercial viability. This well-established precedent minimizes the impact of an academic CAPEX/OPEX evaluation, particularly as site-specific data from commercial processes are not publicly available, and underscores that a detailed technoeconomic analysis exceeds the primary scope of this paper, which focuses on the successful extraction of native-like cutin.

A key feature of SCWH is that the high operating temperatures offer substantial opportunities for energy integration. When cooling or depressurizing the reactor, residual heat can be recovered and reused, mitigating overall energy demands. Previous research even indicates that SCWH, if paired with a gas turbine, can result in a self-sustaining energy system.[52] In such a configuration, the heat and power required to maintain supercritical conditions are largely offset by the turbine's recovery of thermal energy, potentially achieving near net-zero external energy input.

Additionally, the extremely short reaction times (≈ seconds) inherent to SCWH are central to its scalability and process
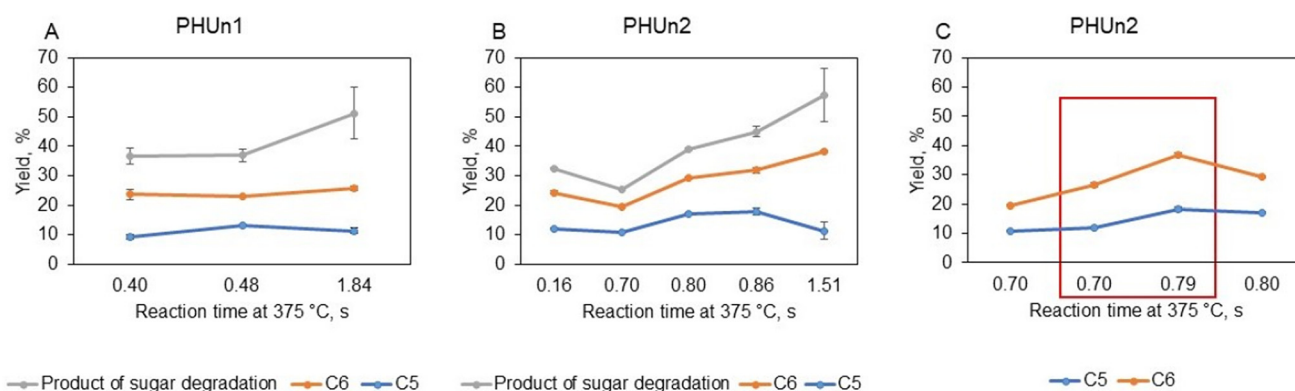


**Fig. 11** The yield of C5, C6, and product of sugar degradation for experiments done on PhUN1 (A), on PhUN2 (B) and comparison of yields for experiments without and with the addition of acetic acid-framed (C).

intensification potential. High temperatures and rapid hydrolysis kinetics not only drastically reduce the reactor volume required but also enable continuous, compact tubular reactor designs. These are straightforward to install and operate at larger scales while minimizing both capital (CAPEX) and operational (OPEX) expenses. Notably, the European Federation of Chemical Engineers (EFCE) has recognized this reactor concept for its innovative Process Intensification approach,[53] underscoring its industrial relevance. The short residence times facilitate efficient heat integration (*e.g.*, reuse of residual heat upon cooling/depressurization), support near net-zero external energy input when paired with gas turbine systems, and yield minimal solvent usage, given that pure water is the only fluid involved. This synergy of design factors, high temperature, compact footprint, and industrial validation, reinforces SCWH as a viable, sustainable method for producing native-like cutin at commercially significant scales.

Furthermore, the process fluid in SCWH is just water, eliminating the need for hazardous chemicals and reducing solvent-handling overheads. After hydrolysis, the aqueous streams can be evaporated with the reactor's residual heat, allowing the water to be readily recycled, or even purified for reuse, thereby lowering both water usage and overall operational costs.

Although a comprehensive life-cycle assessment (LCA) is beyond our immediate scope, we acknowledge that thorough sustainability analyses (energy sourcing, carbon footprint, byproduct management) are vital for evaluating SCWH's full environmental impact. Our prior findings, as well as studies from other supercritical technologies, suggest that heat recovery strategies and minimal chemical inputs can make SCWH environmentally and economically advantageous compared to conventional hydrolytic methods.

Finally, the SCWH process yields co-products such as hydrolyzed C5 and C6 sugars, which can be fermented or converted into platform chemicals, thereby maximizing the overall value stream. Residual solids, like tomato seeds, may also find application in bioenergy or specialty product sectors. Altogether, SCWH's compact reactor design, rapid processing capabilities, and potential self-sufficiency underscore its strong fit for large-scale biomass valorization, paving the way for deeper LCA-based sustainability and technoeconomic studies in the future.

## 4. Conclusions

Supercritical water hydrolysis effectively produces cutin-rich solids from tomato peels waste, presenting a promising method for the valorizing of agricultural residues. This study demonstrates that SCWH preserves the native three-dimensional polyester network of cutin, maintaining its maintaining its structural integrity. Multiple analyses support this finding: FTIR identified characteristic ester bonds bands, DSC showed no melting transitions indicative of monomeric cutin, and mechanical analysis revealed relatively high rigidity due to the preserved cross-linked structure.

The investigation of reaction time revealed that a duration exceeding 1 second are necessary to achieve complete removal of carbohydrates; however, longer reaction times may lead to partial hydrolysis of cutin and increase the extractives fraction. Particle size distribution analysis indicated a median particle size of approximately 20 μm for cutin-rich solids, with smaller fractions corresponding to residual carbohydrates.

The successful preservation of cutin's native structure, coupled with optimized SCWH conditions, underscores the feasibility of this method for producing high-quality cutin-rich materials. These findings contribute to sustainable biomass processing techniques and offer opportunities for developing bio-based materials from agricultural waste streams. Further research could enhance the efficiency and scalability of SCWH processes, facilitating the advancement of sustainable materials and reducing reliance on fossil-fuel-derived polymers.

## Author contributions

## Data availability

The data are in the submitted manuscript. For additional details mail to corresponding author.

## Conflicts of interest

Authors declare that they have no conflict of interest.

## Acknowledgements

# References

1 S. Chatterjee, S. Sarkar, J. Oktawiec, Z. Mao, O. Niitsoo and R. E. Stark, *J. Visualized Exp.*, 2012, 1–7.

2 E. A. Fich, N. A. Segerson and J. K. C. Rose, *Annu. Rev. Plant Biol.*, 2016, **67**, 207–233.

3 V. Zeisler-Diehl, Y. Müller and L. Schreiber, *J. Plant Physiol.*, 2018, **227**, 66–74.

4 E. Domínguez, J. Cuartero and A. Heredia, *Plant Sci.*, 2011, **181**, 77–84.

5 A. Heredia, J. J. Benítez, A. González Moreno and E. Domínguez, *New Phytol.*, 2024, **244**, 65–73.

6 J. A. Heredia-Guerrero, J. J. Benítez, E. Domínguez, I. S. Bayer, R. Cingolani, A. Athanassiou and A. Heredia, *AIP Conf. Proc.*, 2016, **28**, 10–13.

7 I. Lara, A. Heredia and E. Domínguez, *Front. Plant Sci.*, 2019, **10**, 770.

8 Food and Agriculture Statistics | FAO | Food and Agriculture Organization of the United Nations, **https://www.fao.org/food-agriculture-statistics/en/**, (accessed 8 April 2024).

9 E. Elbadrawy and A. Sello, *Arabian J. Chem.*, 2016, **9**, S1010–S1018.

10 D. Shao, G. G. Atungulu, Z. Pan, T. Yue, A. Zhang and X. Chen, *Trans. ASABE*, 2013, **56**, 261–268.

11 G. Rossini, G. Toscano, D. Duca, F. Corinaldesi, E. Pedretti and G. Riva, *Biomass Bioenergy*, 2013, **51**, 177–182.

12 J. J. Benítez, P. M. Castillo, J. C. del Río, M. León-Camacho, E. Domínguez, A. Heredia, S. Guzmán-Puyol, A. Athanassiou and J. A. Heredia-Guerrero, *Materials*, 2018, **11**, 1–13.

13 C. J. S. Moreira, A. Bento, J. Pais, J. Petit, R. Escórcio, V. G. Correia, Â. Pinheiro, Ł. P. Haliński, O. O. Mykhaylyk, C. Rothan and C. Silva Pereira, *Plant Physiol.*, 2020, **184**, 592–606.

14 M. B. Gómez-Patiño, R. Estrada-Reyes, M. E. Vargas-Diaz and D. Arrieta-Baez, *Polymers*, 2020, **12**(9), 1945.

15 M. J. Cocero, Á. Cabeza, N. Abad, T. Adamovic, L. Vaquerizo, C. M. Martínez and M. V. Pazo-Cepeda, *J. Supercrit. Fluids*, 2018, **133**, 550–565.

16 E. Menalla, J. G. Serna, D. Cantero and M. J. Cocero, *Chem. Eng. J.*, 2024, **493**, 152391.

17 D. A. Cantero, M. D. Bermejo and M. J. Cocero, *Bioresour. Technol.*, 2013, **135**, 697–703.

18 D. A. Cantero, M. D. Bermejo and M. J. Cocero, *ChemSusChem*, 2015, **8**, 1026–1033.

19 D. Rigo, T. Fechter, E. Capanema, D. Diment, M. Alopaeus, D. Tarasov, D. Cantero and M. Balakshin, *ChemSusChem*, 2025, **18**(1), e202401683.

20 T. Adamovic, D. Tarasov, E. Demirkaya, M. Balakshin and M. J. Cocero, *J. Cleaner Prod.*, 2021, **323**, 129110.

21 D. A. Cantero, L. Vaquerizo, F. Mato, M. D. Bermejo and M. J. Cocero, *Bioresour. Technol.*, 2015, **179**, 136–143.

22 C. M. Martínez, D. A. Cantero and M. J. Cocero, *J. Cleaner Prod.*, 2008, **204**, 888–895.

23 E. G. Mission and M. J. Cocero, *Green Chem.*, 2022, **24**, 8393–8405.

24 P. T. Anastas and J. B. Zimmerman, *IEEE Eng. Manage. Rev.*, 2007, **35**, 16–16.

25 M. Arshadi, T. M. Attard, R. M. Lukasik, M. Brncic, A. M. Da Costa Lopes, M. Finell, P. Geladi, L. N. Gerschenson, F. Gogus, M. Herrero, A. J. Hunt, E. Ibáñez, B. Kamm, I. Mateos-Aparicio, A. Matias, N. E. Mavroudis, E. Montoneri, A. R. C. Morais, C. Nilsson, E. H. Papaioannou, A. Richel, P. Rupérez, B. Škrbić, M. B. Solarov, J. Švarc-Gajić, K. W. Waldron and F. J. Yuste-Córdoba, *Green Chem.*, 2016, **18**, 6160–6204.

26 A. R. C. Morais, A. M. Da Costa Lopes and R. Bogel-Łukasik, *Chem. Rev.*, 2015, **115**, 3–27.

27 S. Singh, Apoorva, P. Saha, N. Rai, S. Kumari and S. Pandey-Rai, *Ind. Crops Prod.*, 2023, **199**, 116789.

28 G. Philippe, I. Sørensen, C. Jiao, X. Sun, Z. Fei, D. S. Domozych and J. K. Rose, *Curr. Opin. Plant Biol.*, 2020, **55**, 11–20.

29 Y. Shinozaki, P. Nicolas, N. Fernandez-Pozo, Q. Ma, D. J. Evanich, Y. Shi, Y. Xu, Y. Zheng, S. I. Snyder, L. B. B. Martin, E. Ruiz-May, T. W. Thannhauser, K. Chen, D. S. Domozych, C. Catalá, Z. Fei, L. A. Mueller, J. J. Giovannoni and J. K. C. Rose, *Nat. Commun.*, 2018, **9**, 1–13.

30 Pronat, 2024, **https://www.pronat.com.es/en/home-en/**, (accessed 14 October 2024).

31 L. España, J. A. Heredia-Guerrero, P. Segado, J. J. Benítez, A. Heredia and E. Domínguez, *New Phytol.*, 2014, **202**, 790–802.

32 A. Sluiter, B. Hames, R. Ruiz, C. Scarlata, J. Sluiter, D. Templeton and D. Crocker, *Natl. Renewable Energy Lab.*, 2008, **17**, NREL/TP-510-42618.

33 A. Sluiter, B. Hames, D. Hyman, C. Payne, R. Ruiz, C. Scarlata, J. Sluiter, D. Templeton and J. W. Nrel, *Lab. Anal. Proced.*, 2008, **36**, 302–305.

34 A. Sluiter, B. Hames, D. Hyman, C. Payne, R. Ruiz, C. Scarlata, J. Sluiter, D. Templeton and J. W. Nrel, *Natl. Renewable Energy Lab.*, 2008, 3–5.

35 C. M. Martínez, T. Adamovic, D. A. Cantero and M. J. Cocero, *J. Supercrit. Fluids*, 2019, **143**, 242–250.

36 R. Posmanik, D. A. Cantero, A. Malkani, D. L. Sills and J. W. Tester, *J. Supercrit. Fluids*, 2017, **119**, 26–35.

37 Z. Al-Rekabi and S. Contera, *Proc. Natl. Acad. Sci. U. S. A.*, 2018, **115**, 2658–2663.

38 W. Huang, M. Z. Hua, S. Li, K. Chen, X. Lu and D. Wu, *Crit. Rev. Food Sci. Nutr.*, 2024, **64**, 11672–11700.

39 C. Hood, T. Laredo, A. G. Marangoni and E. Pensini, *J. Appl. Polym. Sci.*, 2021, **138**, 50831, DOI: **10.1002/app.50831**.

40 A. Simões, I. M. Coelhoso, V. D. Alves and C. Brazinha, *Membranes*, 2023, **13**, 261.

41 Analyzing Particle Size Distribution Unlocking Insights in Material Science | by Applied technical services | Medium, **https://medium.com/@atslabusa/analyzing-particle-size-**

distribution-unlocking-insights-in-material-science-e6136033172e, (accessed 10 April 2024).

42 J. A. Heredia-Guerrero, J. J. Benítez, E. Domínguez, I. S. Bayer, R. Cingolani, A. Athanassiou and A. Heredia, *Front. Plant Sci.*, 2014, **5**, 1–14.

43 A. S. Sengar, A. Rawson, M. Muthiah and S. K. Kalakandan, *Ultrason. Sonochem.*, 2020, **61**, 104812.

44 J. J. Benítez, A. J. Matas and A. Heredia, *J. Struct. Biol.*, 2004, **147**, 179–184.

45 G. López-Casado, A. J. Matas, E. Domínguez, J. Cuartero and A. Heredia, *J. Exp. Bot.*, 2007, **58**, 3875–3883.

46 A. N. Round, B. Van, S. Dang, R. Estephan, R. E. Stark and J. D. Batteas, *Biophys. J.*, 2000, **79**, 2761–2767.

47 C. J. S. Moreira, A. Bento, J. Pais, J. Petit, R. Escórcio, V. G. Correia, Â. Pinheiro, Ł. P. Haliński, O. O. Mykhaylyk, C. Rothan and C. S. Pereira, *bioRxiv*, 2020, 2020.06.01.127837.

48 G. Tedeschi, J. J. Benítez, L. Ceseracciu, K. Dastmalchi, B. Itin, R. E. Stark, A. Heredia, A. Athanassiou and J. A. Heredia-Guerrero, *ACS Sustainable Chem. Eng.*, 2018, **6**, 14955–14966.

49 V. Leontigevic, D. Cantero and M. J. Cocero, *Of. Española Pat. y Marcas*, 2024, 24382515.

50 D. A. Cantero, C. Martínez, M. D. Bermejo and M. J. Cocero, *Green Chem.*, 2015, **17**, 610–618.

51 Renmatix (USA), **https://renmatix.com/**.

52 D. A. Cantero, L. Vaquerizo, F. Mato, M. D. Bermejo and M. J. Cocero, *Bioresour. Technol.*, 2015, **179**, 136–143.

53 EFCE, EFCE Process Intensification Award.